Proceedings of the 18th International Conference on Nuclear Engineering
ICONE18
May 17-21, 2010, Xi'an, China

ICONE18-29881

ADVANCES IN INVERSE TRANSPORT METHODS

Zeyun Wu
Department of Nuclear Engineering
Texas A&M University
College Station, TX 77840
Email: zeyunwu@hotmail.com

Marvin L. Adams
Department of Nuclear Engineering
Texas A&M University
College Station, TX 77840
Email: mladams@tamu.edu

ABSTRACT

We present advances in inverse transport methods and demonstrate their application to neutron tomography problems that have significant scattering. The problem we consider is inference of the material distribution in an object by detection and analysis of the radiation exiting from it. Our approach combines both deterministic and stochastic optimization methods to find a material distribution that minimizes the difference between computed and measured detector responses. The main advances are dimension-reduction schemes that we have designed to take advantage of known and postulated constraints. One key constraint is that the cross sections for a given region in the object must be the cross sections for a real material. We illustrate our approach using a neutron tomography model problem on which we impose reasonable constraints, similar to those that in practice would come from prior information or engineering judgment. This problem shows that our method is capable of generating results that are much better than those of deterministic minimization methods and dramatically more efficient than those of typical stochastic methods.

INTRODUCTION

A familiar example of an inverse problem in radiation transport is tomography in medical applications, which attempts to reconstruct the interior of a patient from transmitted and reflected radiation collected while illuminating the patient from different directions [1, 2]. We use "inverse transport" and "tomography" to mean the inference of material distribution inside an object based upon detection and analysis of radiation emerging from the object. In many cases, especially when particles are likely to undergo multiple scattering events within the object, inverse problems are ill-conditioned and thus very difficult to solve. This is the class of problems that we address.

One of the more common tomographic techniques is the filtered back projection (FBP) method [1–6]. In this technique, the projection data can be considered as line integrals along the particle beam lines and the tomographic method recovers the density function (the images) by doing back projection process to the filtered Fourier transform of the line integrals. However, for highly scattering objects this method has difficulty because the scattered particles can overwhelm the signal from the unscattered particles. Even with collimated beams and collimated detectors FBP still fails for optically thick, highly scattering problems. We will illustrate this issue with example FBP results in the application section.

We cast the inverse problem as an optimization problem and consider iterative approaches to minimizing a functional that serves as a measure of the difference between the real object and the latest guess (iterate). In this approach, which is not new, a forward model capable of calculating the detector response does so with an initial "guess" of the material distribution in the unknown object. An inverse model then creates a better "guess" of the object structure in every iterative loop. The forward model can then be repeated using the more accurate guess. This process continues until the determined material distribution minimizes the functional that characterizes the difference between predicted and measured results.This is the fundamental concept behind the model-based iterative imaging reconstruction (MOBIIR) schemes. MOBIIR schemes mainly differ in their choice

Copyright © 2010 by ASME

of forward model and how the spatial distributions of the optical properties of the medium are updated.

A variety of optical tomography methods based on MOBIIR schemes have been studied in the past [7–15]. While these studies have principally been in the area of low-energy x-ray medical imaging, they have led to a variety of creative methods and their general application can be extended to neutron imaging. We present here a methodology that combines both deterministic and stochastic iterative methods within a systematic approach for applying constraints. The constraints can enforce physical realities as well as postulates about the contents of the object. Our approach dramatically reduces the effective dimension of the parameter space that is ultimately searched, which dramatically decreases computational effort and increases the chance of a solution that is close to reality.

To illustrate our methodology we consider problems described by a two-dimensional X-Y Cartesian coordinate system. We assume an incident beam of thermal neutrons from one side of the object at a time, with measurement of exiting radiation from the other three sides. Our forward solver employs a single (thermal) energy group, the discrete-ordinates method for angular discretization, an analytic treatment of the first-collision source, and the step-characteristic method for spatial discretization. In this paper we do not consider the complications of model or measurement errors - our aim here is to evaluate whether our methodology works in a simple setting that permits sharp analysis and sharp conclusions.

In the following section we introduce our procedure, highlighting the ideas that we believe are new. In Section 3 we present results from an illustrative model problem. In the final section we offer some concluding remarks.

INVERSE TRANSPORT METHODS

Neutron transport within a non-multiplying object is described by the transport equation:

$$\begin{gathered}\underline{\Omega} \bullet \psi(\underline{r},\underline{\Omega}) + \Sigma_t(\underline{r})\psi(\underline{r},\underline{\Omega}) = \\ \frac{1}{4\pi}\Sigma_s(\underline{r})\left[\phi(\underline{r}) + 3g(\underline{r})\underline{\Omega} \bullet \underline{J}(\underline{r})\right] + S_{ext}(\underline{r},\underline{\Omega}).\end{gathered} \tag{1}$$

Where Σ_t and Σ_s are the total and scattering macroscopic cross sections and g denotes the average cosine of the scattering angle. (We have assumed linearly anisotropic scattering.) These three functions are determined by the material composition of the object.

The forward transport problem is to solve for the angular flux ψ (which determines the scalar flux ϕ and current $\underline{J}$) if the physics constants (Σ_t, Σ_s, g) are provided as functions of position. In an inverse transport problem, on the contrary, the usual task is to infer the material distribution within the object based on the limited information about that is obtained from detections of exiting radiation. Most methods for solving such problems have focused on inferring Σ_t, Σ_s and g from the detection measurements and have not explicitly addressed the issue of inferring material distribution from these constants. In contrast, a key feature of our approach is that we treat the *material* as our unknown function of position, as we describe in more detail below.

We cast the inverse transport problem as an optimization problem, the goal of which is to minimize an objective function:

$$\Phi = \frac{1}{2}\sum_{i=1}^{N}\left(\frac{P_i - M_i}{M_i}\right)^2. \tag{2}$$

Here Φ denotes the objective function, P and M are the predicted and measured detection rates, respectively, and N is the total number of measurements taken. The predicted values, and thus the objective function, depend on the functions $\Sigma_t(\underline{r})$, $\Sigma_s(\underline{r})$, and $g(\underline{r})$, which in turn depend on a guess for the distribution of materials in the object. The key ingredient in the optimization algorithm is the method for intelligently guessing material distributions for which the forward transport problem will be solved and the resulting objective function will be computed.

Deterministic optimization methods minimize the objective function in Eqn. (2) by treating the measurements P_i, and thus the objective function Φ, as functions of the parameters $\{\Sigma_t(\underline{r}), \Sigma_s(\underline{r}), g(\underline{r})\}$. The goal then becomes finding a set $\{\Sigma_t(\underline{r}), \Sigma_s(\underline{r}), g(\underline{r})\}$ such that the objective function is minimized. Our method uses this approach but only as a first step in a hierarchical multi-step algorithm. For this step we follow the basic approach of Klose et al. [14, 15] as corrected by Scipolo [16], with some improvements that we shall summarize briefly below.

As the modeling of the problem becomes more realistic, the number of unknown parameters (spatial and energy-dependent cross sections) increase drastically, which makes the optimization problem far more difficult to solve. The dimension of the search space is the number of spatial regions (cells) times the total number of unknown cross sections, which in a neutron scattering problem scales as the square of the number of energy groups or energy points. The large number of unknowns (high-dimensional space) makes the problem more ill-conditioned and dramatically increases the number of iterations needed to find a minimum. Further, in practice it is highly unlikely that the set of parameters found in a given cell by the search algorithm will correspond to any real material. Thus, even if a set of parameters is found that yields an acceptably small objective function, the end goal of determining the material distribution in the object may remain difficult to achieve.

These considerations motivate us to consider our problem from a different point of view. Instead of viewing the unknowns as *cross sections*, we view the unknowns as the *material* itself. This reduces the number of unknowns from a large number per

Copyright © 2010 by ASME

cell to only one per cell. However, it changes the nature of the problem and thus the methodologies needed to solve it. The unknowns are now discrete (the material index in a given spatial cell) instead of continuous (a real number for a given cross section in a given cell). Now we cannot take meaningful derivatives of the objective function with respect to an unknown and thus cannot apply gradient-based minimization approaches. In fact, the problem now can be viewed as a combinatorial optimization (CO) problem. Such problems are usually solved by stochastic-based heuristic approaches. In such an approach, examples of which include simulated annealing and genetic algorithms, guesses for the solution (material index for each spatial cell) are generated using random numbers coupled with some information learned from previous guesses.

When we evaluate the direct application of standard CO methods (TABU search, simulated annealing, genetic algorithms, etc.) to our problem we find that the dimensionality of the problems of interest is so high that the methods are not likely to produce results with sufficient efficiency for practical use. The number of possible combinations is the number of candidate materials raised to the power of the number of spatial cells. For example, if prior knowledge suggests that the object contains nothing outside of a list of 10 known materials and the desired resolution of the distribution is $15 \times 15 \times 15 = 3375$ spatial cells, then there are 10^{3375} potential distributions to evaluate. Thus, while we have dramatically reduced the number of degrees of freedom by choosing *material* (instead the large number of multigroup cross sections) as our unknown in each cell, to obtain a practical method we must achieve further significant reductions in the number of degrees of freedom.

We have devised a multi-step algorithm to accomplish this goal. The algorithm proceeds as follows:

1. **Gradient-based deterministic search:** Here we apply the basic deterministic search algorithm, in which cross-section parameters are the unknowns. However, we employ a simplified transport model (for example one-group or two-group transport or diffusion), perhaps on a spatial grid that is not as fine as the ultimate desired resolution. Thus, the dimension of the search space is manageable.

2. **Cell Grouping:** Based on the results from the deterministic optimization process, we group into *regions* the cells that are likely to contain the same material. Another kind of region is identified as likely to contain one or more interfaces between materials. Henceforth each cell will be associated with a region, with materials varying by region according to some chosen constraints (see step 4). After this grouping, the forthcoming search process will work on regions rather than cells, which greatly reduces the search-space dimension and thus greatly saves computation time.

3. **Material Restriction:** The purpose of this step is to narrow the material candidates to be considered in each region. Given the few-group parameters found in step 1 for the cells in a given region, an algorithm determines which materials could realistically have few-group parameters that are similar, and then places those materials in the material candidate library (MCL) for that region.

4. **Further Constraints:** To further reduce the search space we can impose other constraints that embody prior knowledge or that are postulated. For example, we could constrain the algorithm to consider only material sub-objects with relatively sharp boundaries as opposed to fragmentary objects. We could bias the stochastic search process so that it favors a small number of material regions embedded in a single-material background. The chosen constraints restrict the kinds of material distributions that will be considered as viable candidates in the final step.

5. **Stochastic-based Combinatorial Optimization:** In this stage we produce a sequence of guesses for the material distribution and compute the objective function for each guess. We apply a stochastic-based heuristic search method, informed by the constraints and biases chosen in step 4, to select a material in each cell. At this stage a full-fidelity transport forward model is applied to evaluate the objective function for each material distribution. The algorithm terminates either when a suitably small objective function is found or when an iteration limit is reached.

We remark that we have implemented several improvements to the approach described by Klose et al. [14, 15] and corrected by Scipolo [16]. First, we perform a variable change to impose non-negativity constraints on cross sections; this is described in a forthcoming publication [17]. To increase efficiency we apply a Krylov subspace iterative technique that speeds up each forward calculation. We employ a nonlinear conjugate gradient (CG) [18] updating scheme as the heart of our search procedure and integrate Brent's method [19] into the associated line-search algorithm. We also allow illumination of the object from all four sides of a rectangular object in 2D, with each illumination producing a set of measurements. All four sets are included in the sum that defines the objective function.

The following section demonstrates our algorithm by applying it to a model problem that contains significant scattering.

APPLICATIONS TO TOMOGRAPHY

We consider a model problem with two materials inside an object, with an "inclusion" of one material embedded in a "background" of another material. Fig. 1 is a schematic diagram for the problem.

Copyright © 2010 by ASME

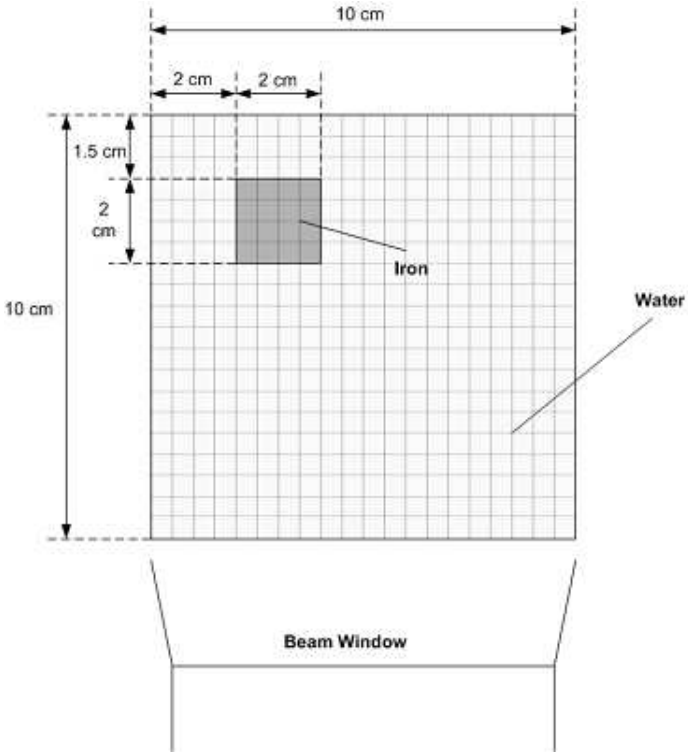

Figure 1. Schematic diagram of the test problem

Table 1. Material properties

Material	Water	Iron
Σ_s (1/cm)	0.7362	0.9672
Σ_t (1/cm)	0.7435	1.1788
g	0.037	0.012
Σ_{tr} (1/cm)	0.7163	1.1672
mfp(cm)	1.345	0.8483
c	0.9902	0.8204

Table 1 lists the properties of the materials in the test problem. The transport cross section (Σ_{tr}), mean free path (*mfp*) and scattering ratio (c) are deduced properties which are defined as:

$$\Sigma_{tr} = \Sigma_t - g\Sigma_s, \quad mfp = \frac{1}{\Sigma_t}, \quad c = \frac{\Sigma_s}{\Sigma_t}. \tag{3}$$

We list these three properties because they are usually considered important and useful characteristics of the physical problem. For example, by observing the magnitude of *mfp* and c, we may state that our test problem is optically thick and highly scattering. We will use Σ_{tr} as a representative factor to infer material distribution in our example problem.

We have attempted to solve this problem with a traditional direct tomography tool, i.e., a filtered back projection (FBP) method. To give the FBP method the best possible chance to succeed, we employed collimated beams and collimated detectors. However, even with collimation, if a problem is sufficiently thick and highly scattering the scattered particles will contribute more to the detector signal than will the directly transmitted particles. This is the case with our test problem. This violate the fundamental assumption behind FBP, and thus the method fails to find the inclusion. If we repeat this exercise with all dimensions reduced by a factor of five, then FBP does indeed find the inclusion.

Our interest in this paper is in problems, such as the one shown in Fig. 1, that are too thick and highly scattering for techniques such as FBP. The general methodology that we described in the previous section is our attempt to address such problems. Here we apply this general methodology to the test object of Fig. 1, with the following specific choices:

1. Our forward transport model is a one-group equation with linearly anisotropic scattering in both the first and last steps. In the first step we use a spatial grid of 20×20 cells; in the final step we use 40×40 cells. (The methodology permits an even higher-fidelity model in the last step, but we want to keep this initial demonstration simple.)

2. We use the same model with the exact material distribution to generate the "measurements" and we do not add any noise. A practical algorithm must deal with noise, and there are established methods for doing so, but again we wish to keep this demonstration simple.

3. We employ a cell-grouping algorithm that assumes a single inclusion in a background of a single material. It divides the domain into three regions: background, inclusion, and interface.

4. We begin with a small MCL of ten materials. In addition to water and iron, the library includes paraffin, boron, silicon, nitrogen, cadmium, aluminum, natural uranium and high enriched uranium (HEU). For all ten materials we used thermal cross sections averaged with a roughly-Maxwellian spectrum.

5. We impose constraints that enforce a single inclusion in a background of a single material. We do not allow the interface to be arbitrarily ragged; for example, a "finger" of one material that is one cell wide is not permitted to extend into the other material to a depth beyond one cell. We

Copyright © 2010 by ASME

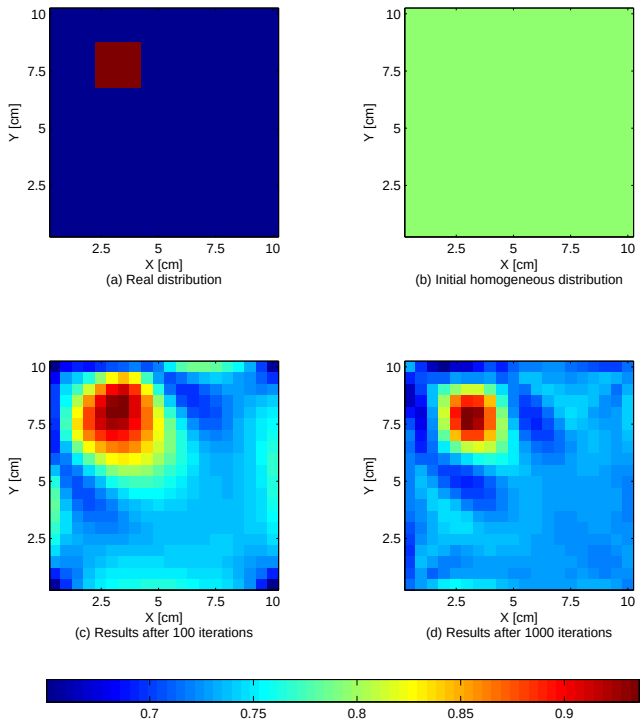

Figure 2. Transport cross section (Σ_{tr}) distribution obtained from deterministic CG based iterative search scheme. (a) The real Σ_{tr} (background is water and square inclusion is iron). (b) Initial guess for Σ_{tr}. (c) and (d) are results after 100 and 1000 iterations, respectively.

employ bias in the stochastic material-choice algorithm for the interface region, such that a cell close to the inclusion region is more likely to be assigned the inclusion material and a cell close to the background region is more likely to be assigned the background material.

6. The stochastic method employed in the final step is extremely simple. Each guess is determined independently from all other guesses (no learning is attempted), using random numbers for each degree of freedom. The biasing described above is employed, the constraints described above are imposed.

Fig. 2 illustrates the results from the first step (gradient-based search for cross sections and g factor). Fig. 2(a) is just the real Σ_{tr} distribution of the problem as shown in Fig. 1, we repeat it here just for comparison purpose with it to our optimized results. We start the deterministic optimization process with a homogeneous material distribution (see Fig. 2(b)). And Fig. 2(c) and (d) are the Σ_{tr} distribution among the object yielded from the process of updating schemes of our inverse model. We expect the more accurate results as the more iterates carried on. We see that the gradient-based continuous search process indicates that there is an inclusion and roughly tells its location after 1000 iterations. By this stage we have the similar outcome for parameters Σ_t and g as well in our inverse problem though we only demonstrate Σ_{tr} as an representative in Fig. 2.

We may use these information to indicate the real physical material in the object and in fact many traditional tomography methods did work out problems in this way. However, there are significant drawbacks associated with this approach. For example, the converged cross sections always have deviations from the real ones and they are not constrained to be realistic there forth may not correspond to any real material. In addition, it is usually difficult to tell which material is inside the object from this limited information, and it is also difficult to locate the boundary and thus quantify how much area is occupied by the inclusion. The following contents we are about to present in this paper is attempting to overcome these drawbacks.

Here we emphasize that we would continue our process by working on *materials* themselves rather than *cross sections*. First we group the cells based on the knowledge gained from the first stage. We devise a criterion to divide the problem into different regions. Many criteria are possible; for this model problem we set up the following simple criterion as:

$$\begin{aligned} &\Sigma_{tr} > \Sigma_{tr}^{mean} + \alpha(\Sigma_{tr}^{max} - \Sigma_{tr}^{mean}) \Rightarrow \text{ Region 3 (inclusion)} \\ &\Sigma_{tr} < \Sigma_{tr}^{mean} + \beta(\Sigma_{tr}^{max} - \Sigma_{tr}^{mean}) \Rightarrow \text{ Region 1 (background)} \\ &\text{otherwise } \Rightarrow \text{ Region 2 (interface)}, \end{aligned} \tag{4}$$

we use $\alpha = 0.8$, $\beta = 0.2$ in our demonstration.

The result of cell grouping is illustrated in Fig. 3. By far we successfully group the cells of our problem into 3 regions: background region (region 1), interface region (region 2) and inclusion region (region 3).

The next step is to restrict the material candidates in the inclusion and background regions by comparing cross sections of each material in MCL to the cross sections that were found in the deterministic search process. We first calculate an *error* associated with each material for each region. Many "error" metrics and restriction criteria are possible; for this illustration we have chosen the following metric:

$$e_m = error = \frac{1}{3}\left(\left|\frac{\Sigma_s^m - \Sigma_s^r}{\Sigma_s^m + \Sigma_s^r}\right| + \left|\frac{\Sigma_t^m - \Sigma_t^r}{\Sigma_t^m + \Sigma_t^r}\right| + \left|\frac{\Sigma_{tr}^m - \Sigma_{tr}^r}{\Sigma_{tr}^m + \Sigma_{tr}^r}\right|\right). \tag{5}$$

Here Σ^m is the cross section of a given material in MCL and Σ^r is cross section averaged over the inclusion/background region. We restrict the material candidates for the region based on the following criterion: if there exists one and only one material that has $e_m < a$, the region is determined to be that material m; i.e., we find the material in the region. Otherwise we include all materials for which $e_m < b$. Here a is a relatively small number and b is a relatively larger number; for this illustration we use

Copyright © 2010 by ASME

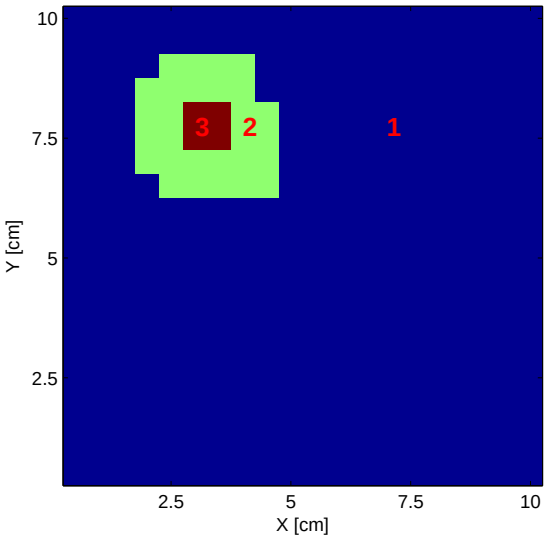

Figure 3. Regions identified by the cell grouping process (color denotes region, not any particular numerical value).

$a = 0.01$, $b = 0.5$. At the end of this stage we have significantly reduced the material search dimension for the final step.

The final step is the combinatorial optimization process. A single iteration in this step proceeds as follows. First the material in the inclusion region is selected from the restricted set of candidates, as is the material in the background region. For this test problem our algorithm determined that the background material must be water; thus region 1 was always chosen to be water. Our algorithm determined that the inclusion could be any one of four different materials: iron, water, paraffin, natural uranium. (Implementation detail: instead of randomly selecting the inclusion material for each iteration, which would have apportioned roughly 25% of the iterations to each candidate material, we deterministically assigned 25% of the iterations to each candidate material.) With water assigned to region 1 and a choice made for region 3, the algorithm proceeded to assign one of these two materials to each cell in the interface region (region 2).

The assignment began with the cells adjacent to region 3 and marched out to those adjacent to region 1, proceeding as follows. For each cell in the inner ring the material was chosen based on a random number and a bias factor. The probability that the inclusion material was assigned to a cell was approximately the cell's distance to region 1 divided by the distance from region 3 to region 1. After materials were assigned to the inner ring of interface-region cells we checked whether the assignments for other interface-region cells were determined by defined constraints. For example, if water were assigned to an entire row of cells, then all interface cells between that row and the water region must also be water - otherwise the inclusion region would be disjoint or more ragged than permitted by the imposed constraint. This greatly reduced the number of allowed configurations and avoided time-consuming calculations of unrealistic distributions.

The results of applying this algorithm are shown in Fig. 4 and quantitatively assessed in Table 2. With only 200 random guesses (50 for each candidate inclusion material), the configuration shown in the figure was found and selected as the best of the 200 distributions because it had the lowest objective function. The graphical solution is strikingly similar to the correct distribution, but more important is the quantitative comparison shown in Table 2. Here we find that the method produces *exactly the correct mass* (area corresponds to mass) of the *correct material* and almost exactly the *correct center-of-mass location*. This is exactly what one would like to get from a neutron tomography method.

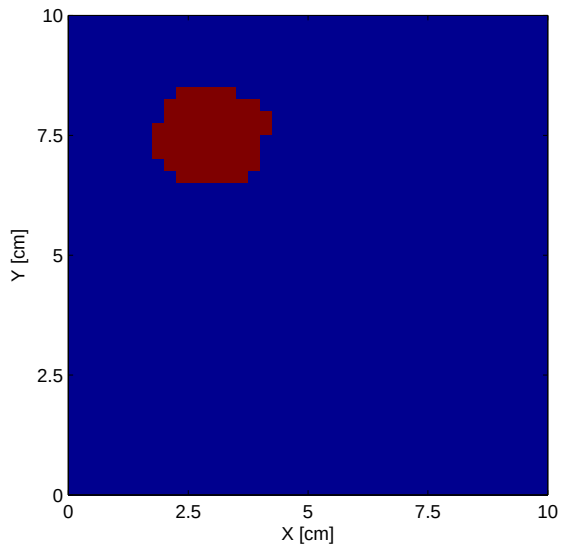

Figure 4. Material distribution yields from the stochastic based heuristic optimization after 200 iterations (50 iterations per candidate inclusion material).

Table 2. Inclusion material location and area comparison

Case	Real (Fig. 2a)	CO Result (Fig. 4)
X-center (cm)	3.0	2.97
Y-center (cm)	7.5	7.49
Area (cm^2)	4.0	4.0
Iron/Water	0.0417	0.0417

Copyright © 2010 by ASME

CONCLUSIONS

We have introduced some advances in inverse transport methods and applied them to solve 2D neutron tomography problems. Our main idea is to employ multiple steps that work together to dramatically reduce the difficulty of the combinatorial optimization problem that ultimately produces an estimate of the material distribution in the object being investigated. The steps implement a series of novel dimension-reduction techniques and integrate them to achieve the desired result.

Results from a simple model problem illustrate the potential power of these ideas. An optically thick problem with a high scattering ratio is solved almost exactly with very modest computational effort, as described in the previous section.

Our main ideas and overall step-by-step approach leave room for considerable exploration and innovation that could improve on what we have shown and expand its applicability. We have made simple choices here for constraints and biases; these could surely be improved and placed on firmer theoretical footing. We have ignored the issues of measurement noise and model error, both of which must be addressed in any practical method; there are proven methods for this, but it remains to be shown that they can be employed within our framework. We have not discussed constraints that could be imposed in problems with more than two materials or more than one inclusion; straightforward generalizations of this paper's constraints are possible, but there may be superior approaches. Further work is needed on algorithms for restricting materials based on results from the deterministic search. In practical applications the search may use a crude few-group model and thus produces few-group cross sections, but each material is actually characterized by energy-dependent or many-group cross sections. In the absence of known weighting spectra it is not clear how to compare the few-group cross sections with the real material cross sections. Thus, we believe the approach that we have outlined and illustrated here is very promising, but much work remains before it can be applied to practical problems.

REFERENCES

[1] Kak, A. C., and Slaney, M., 1987. *Principles of Computerized Tomogrphic Imaging*. IEEE Press.

[2] Herman, G. T., 1980. *Image Reconstruction from Projections*. Academic Press.

[3] Vainberg, E. I., Kazak, I. A., and Kurozaev, V. P., 1981. "Reconstruction of the internal three-dimensional structure of objects based on real-time internal projections". *Soviet J. Nondestructive Testing,* ***17***, pp. 415–423.

[4] Smith, K. T., and Keinert, F., 1985. "Mathematical foundations of computed tomography". *Applied Optics,* ***24***, pp. 3950–3957.

[5] Kuchment, P., Lancaster, K., and Mogilevskaya, L., 1995. "On local tomography". *Inverse Problems,* ***11***, pp. 571–589.

[6] Faridani, A., 2003. "Introduction to the mathematics of computed tomography". *Inside Out: Inverse Problems, MSRI Publications,* ***47***.

[7] Jiang, H., and et al., 1995. "Optical image reconstruction using dc data: Simulations and experiment". *Journal of the Optical Society of America A,* ***13***, pp. 253–266.

[8] Davies, A. J., and et al., 1997. "Reverse differentiation and the inverse diffusion problem". *Advances in Engineering Software,* ***28***, pp. 217–221.

[9] Zhou, Z., Leahy, R. M., and Qi, J., 1997. "Approximate maximum likelihood hyperparameter estimation for gibbs priors". *IEEE Transacton on Image Processing,* ***6(6)***, pp. 844–861.

[10] Arridge, S., and Schweiger, M., 1998. "A gradient-based optimisation scheme for optical tomography". *Optics Express,* ***2(6)***, pp. 213–226.

[11] Saquib, S., and et al., 1998. "Ml parameter estimation for markov random fields with applications to bayesian tomography". *IEEE Transaction on Image Processing,* ***7(7)***, pp. 1029–1040.

[12] Hielscher, A., and et al., 1999. "Gradient based iterative image reconstruction scheme for time-resolved optical tomography". *IEEE Transaction on Medical Imaging,* ***18(3)***, pp. 262–271.

[13] McCormick, N., 1999. "Inverse problems for biomedical characterization and imaging". In 3rd Int. Conf. on Inverse Problems in Engineering: Theory and Practice. Port Ludlow, Washington, June 13-18.

[14] Klose, A. D., and et al., 2002. "Optical tomography using the time-independent equation of radiative transfer - part 1: Forward model". *J. Quantitative Spectroscopy and Radiative Transfer,* ***72***, pp. 691–713.

[15] Klose, A. D., and et al., 2002. "Optical tomography using the time-independent equation of radiative transfer - part 2: Inverse model". *J. Quantitative Spectroscopy and Radiative Transfer,* ***72***, pp. 715–732.

[16] Scipolo, V., 2004. "Scattered neutron tomography based on a neutron transport problem". Master's thesis, Texas A&M University.

[17] Wu, Z., and Adams, M. L., 2010. "Variable change technique applied in constrained inverse transport applications". Submitted to American Nuclear Society (ANS) Summer Annual Meeting, San Diego, CA, June 13-17.

[18] Shewchuk, J. R., 1994. An introduction to the conjugate gradient method without the agonizing pain. unpublished paper.

[19] Brent, R., 1973. *Algorithms for Minimization without Derivatives*. Prentice-Hall.

Copyright © 2010 by ASME